ORIGINAL PAPER



Arterial wall thickening normalizes arterial wall tension with growth in American alligators, *Alligator mississippiensis*

Renato Filogonio¹ · Benjamin D. Dubansky² · Brooke H. Dubansky³ · Tobias Wang⁴ · Ruth M. Elsey⁵ · Cléo A. C. Leite¹ · Dane A. Crossley II²

Received: 1 September 2020 / Revised: 21 January 2021 / Accepted: 28 January 2021 © The Author(s), under exclusive licence to Springer-Verlag GmbH, DE part of Springer Nature 2021

Abstract

Arterial wall tension increases with luminal radius and arterial pressure. Hence, as body mass (M_b) increases, associated increases in radius induces larger tension. Thus, it could be predicted that high tension would increase the potential for rupture of the arterial wall. Studies on mammals have focused on systemic arteries and have shown that arterial wall thickness increases with M_b and normalizes tension. Reptiles are good models to study scaling because some species exhibit large body size range associated with growth, thus, allowing for ontogenetic comparisons. We used post hatch American alligators, Alligator mississippiensis, ranging from 0.12 to 6.80 kg (~60-fold) to investigate how both the right aortic arch (RAo) and the left pulmonary artery (LPA) change with M_b . We tested two possibilities: (i) wall thickness increases with M_b and normalizes wall tension, such that stress (stress = tension/thickness) remains unchanged; (ii) collagen content scales with M_b and increases arterial strength. We measured heart rate and systolic and mean pressures from both systemic and pulmonary circulations in anesthetized animals. Once stabilized alligators were injected with adrenaline to induce a physiologically relevant increase in pressure. Heart rate decreased and systemic pressures increased with M_b ; pulmonary pressures remained unchanged. Both the RAo and LPA were fixed under physiological hydrostatic pressures and displayed larger radius, wall tension and thickness as M_b increased, thus, stress was independent from M_b ; relative collagen content was unchanged. We conclude that increased wall thickness normalizes tension and reduces the chances of arterial walls rupturing in large alligators.

Keywords Arterial wall stress · Crocodilians · Law of Laplace · Scaling

Abbreviations

 $f_{\rm H}$ Heart rate

LPA Left pulmonary artery

 $M_{\rm b}$ Body mass

Communicated by G. Heldmaier.

Renato Filogonio renatofilogonio@gmail.com

Published online: 24 February 2021

- Department of Physiological Sciences, Federal University of São Carlos, São Carlos, SP 13565-905, Brazil
- Department of Biological Sciences, Developmental Integrative Biology Cluster, University of North Texas, Denton, TX 76203-5220, USA
- Department of Medical Laboratory Sciences and Public Health, Tarleton State University, Fort Worth, TX, USA
- Section for Zoophysiology, Department of Biosciences, Aarhus University, 8000 Aarhus C, Denmark
- Louisiana Department of Wildlife and Fisheries, Rockefeller Wildlife Refuge, Grand Chenier, LA 70643, USA

Pm_{pul} Pulmonary mean arterial pressure
 Pm_{sys} Systemic mean arterial pressure
 Ps_{pul} Pulmonary peak systolic pressure
 Ps_{sys} Systemic peak systolic pressure
 RAo Right aortic arch

RAo Right aortic arch $r_{\rm i}$ Internal radius T Arterial wall tension W Arterial wall thickness σ Arterial wall stress

Introduction

Blood flows in major arteries increase with body mass (M_b) , and the widening of the arterial internal luminal radius (r_i) needed to accommodate the higher flows is coupled to an increase in arterial wall tension (T—Wolinsky and Glagov 1967; Holt et al. 1981; West et al. 1997; Dawson 2001; Prim et al. 2018; Seymour et al. 2019). This can be described by the Law of Laplace, where wall tension is the product



of luminal internal radius and arterial pressure. It remains debated whether arterial pressure increases with $M_{\rm b}$ in mammals (White and Seymour 2014; Poulsen et al. 2018), but pressure clearly increases with $M_{\rm b}$ in the reptile species studied so far (Seymour 1987; Enok et al. 2014).

The rise in wall tension with increased M_b is typically accompanied by the thickening of the vessel wall (Wolinsky and Glagov 1967; Prim et al. 2018). The relationship between wall tension and wall thickness (W) is known as arterial wall stress ($\sigma = r_i \times P/W$), and corresponds to the normalized wall tension by cross-sectional area of the arterial wall (Wolinsky and Glagov 1967; Shadwick 1998; Seymour and Blaylock 2000; Prim et al. 2018). The composition of the arterial wall, such as the collagen content, could also play an important role strengthening and stiffening the arterial wall (Nichols et al. 2011).

Studies on the scaling of arterial mechanics have focused on interspecific comparisons of the systemic arteries in mammals with different M_b (e.g., Wolinsky and Glagov 1967; Cox 1978; Prim et al. 2018). Reptiles, on the other hand, allow ontogenetic investigations of scaling relationships because many species exhibit large changes in M_b over their life history without substantial changes in overall morphology (Avery 1994), which reduces putative variations resulting from interspecific comparisons (Enok et al. 2014). Here, we investigated whether wall thickness and collagen content from both systemic and pulmonary arterial vessels of the American alligator, Alligator mississippiensis, scaled with $M_{\rm b}$ to increase the capacity to tolerate larger wall tensions. In contrast to most reptiles, crocodilians possess a complete interventricular septum (White 1976; Alves et al. 2016; Cook et al. 2017; Lima et al. 2020) that allows for generation of different arterial pressures at the systemic and pulmonary circulations (e.g. ~ 8 kPa and 2 kPa, respectively, for the estuarine crocodile, *Crocodylus porosus*—Axelsson et al. 1996). Since pulmonary blood pressure is lower than systemic pressure, and the pulmonary artery is usually thinner than the systemic counterpart (Greenfield and Patel 1962; Greenfield and Griggs 1963; van Soldt et al. 2015; Filogonio et al. 2018), we predicted that the wall tension of the pulmonary circulation should scale with a lesser magnitude.

Materials and methods

Experimental animals

From 2013 to 2017, American alligator (*Alligator mississippiensis*) eggs were harvested from the Rockefeller Wildlife Refuge in Grand Chenier, LA (USA), and transported to the University of North Texas in Denton, TX, USA. Eggs

were incubated at 30 °C as previously described (Joyce et al. 2018; Smith et al. 2019) to ensure all embryos developed as females (Ferguson 1985). After hatching, all animals were transferred to holding tanks (500 l), partially filled with water, at room temperature ranging from 26 to 30 °C and a light regime of 12:12 light:dark cycle. All animals were fed ad libitum four times a week (Mazuri® Crocodilian Diet, Mazuri®, PMI Nutrition International, Brentwood, MO, USA). Food was withheld at least 7 days before experiments. Body mass from 14 juvenile alligators ranged from 0.12 to 6.80 kg, representing an almost 60-fold increment.

Instrumentation

All experiments were conducted in environmental chambers at 30 °C. Anesthesia was induced by placing the alligator's head inside a Ziploc bag (17×15 cm) containing isoflurane-soaked cotton gauze (Isoflo®, Abbott Laboratories, USA). After loss of reflexes, the trachea was intubated to enable ventilation with a tidal volume of 20 ml×kg⁻¹ at a rate of 5-8 breaths × min⁻¹ using a Harvard Apparatus 665 ventilator (Harvard Apparatus, Holliston, MA, USA) with a gas mixture of 2% isoflurane, 21% O₂ and 3% CO₂ (GF-3mp, Cameron Instrument Co., Port Aransas, TX, USA) throughout the surgery (Smith et al. 2019). Local anesthesia (lidocaine 2%; Lidoject, Henry Schein Animal Health, Dublin, OH, USA) was administered subdermally at the incision sites, and a longitudinal incision of 2 cm was made in the left thigh to access the femoral artery for occlusive cannulation with a PE50 catheter filled with heparinized saline (50 UI×ml⁻¹). After closing the incision, alligators were placed in a supine position and a thermocouple was introduced into the cloaca and connected to a microprobe thermometer (BAT-12, Physitemp Instruments, Clifton, NJ, USA) for continuous body temperature monitoring. Subsequently, an incision was made at the ventral midline to open the sternum and expose the major vessels close to the heart. The left pulmonary artery (LPA) was non-occlusively cannulated using the Seldinger technique (Seldinger 1953; Filogonio and Crossley 2019). Briefly, we tapered a PE50 catheter over a 23-gauge needle, which was inserted upstream into the artery. After withdrawing the needle, the catheter was connected to a PE50 cannula filled with heparinized saline (50 UI \times ml⁻¹). This procedure was repeated for the right aortic arch (RAo) of smaller alligators (<3.5 kg; n=8). The cannulas were connected to disposable pressure transducers (ADInstruments model MLT0699, ADInstruments), which were calibrated daily against a static water column. Signals were amplified with a Bridge Amp (ADInstruments). Data were recorded at 100 Hz with a PowerLab® 16/35 data acquisition system connected to a computer



running LabChart Pro[®] software (v.8.2, ADInstruments). Heart rate ($f_{\rm H}$), systemic and pulmonary arterial systolic pressures ($P_{\rm S_{sys}}$ and $P_{\rm S_{pul}}$, respectively), and mean arterial pressures ($P_{\rm m_{sys}}$ and $P_{\rm m_{pul}}$, respectively) were derived from the pulsatile pressure signals. All procedures were approved by the University of North Texas animal ethics committee (UNT-IACUC protocol # 17-001).

Experimental protocol

After instrumentation, the isoflurane was reduced to 1% and the cardiovascular parameters were allowed to stabilize for 30 min, after which pressures were recorded for 10 min. Then, adrenaline (2 $\mu g \times kg^{-1}$) was administered through the systemic catheter to elicit a physiologically relevant rise in arterial pressures by affecting vascular resistances (Galli et al. 2007; Filogonio et al. 2019), thus, inducing higher wall tensions at both the RAo and the LPA.

Upon completion of the experiment, the isoflurane level was raised to 5% for 10 min and the animals were euthanized by an injection of pentobarbital (Euthansol; 150 mg \times kg⁻¹) through the carotid artery. The heart was immediately removed to measure its wet mass to the nearest 0.01 g. A 2-3 cm section from both the RAo (after the bifurcation from the right subclavian) and the LPA (after the curvature out of the myocardium) were removed, and freed from surrounding tissue by gross dissection. Isolated arteries were cannulated, and connected to a manometer to control internal pressure of the arteries. Arterial pressures were achieved by injecting 4% phosphate-buffered formalin through the cannula until pressures reached the correspondent peak systolic pressure measured after adrenaline injection for each animal. At this peak pressure, both ends of the arterial segment were tied with suture lines prior to immersion in buffered formalin for histological processing.

Fig. 1 Histological cross-sectional cuts from the right aortic arch of a 2.20 kg American alligator, Alligator mississippiensis. Picro-Sirius red staining. a-c Photos at bright field showing internal radius and circumference (a), and arterial wall thickness (b). d-f Photos at dark field using circular polarization, where collagen is shown in bright yellow, orange or green. At **c** and **f**: Ad tunica adventitia; Me tunica media. Scale bars: a, d = 1 mm; b, e = 0.5 mm; c,f = 0.1 mm

A Internal radius Wall thickness A/G D F A/G Me

Histology

Samples were dehydrated in ascending ethanol concentrations and embedded in paraffin and stained for collagen content (Dubansky and Dubansky 2018). Briefly, 6 µm serial transverse sections were produced (Microm HM355S, Heidelberg, Germany), mounted on charged slides and stained with Picro-Sirius red (Fig. 1; Dubansky and Dubansky 2018). Arterial cross-sections were imaged using a DP71 digital camera mounted in an Olympus BX51 microscope powered by Olympus DP controller software (Olympus America Inc., Savage, Minnesota, USA). Image analysis of micrographs was completed using ImageJ freeware image analysis program (Schneider et al. 2012). Using tools in ImageJ, we estimated the arterial internal radius (r_i) from the internal circumference (C_i): $r_i = C_i/2\pi$ (Fig. 1a). Arterial wall thickness (W; Fig. 1b) was the mean value of measurements made at four different places from the arterial wall. Arterial wall tension was calculated according to the Law of Laplace for cylinders: $T = r_i \times Ps$, where "Ps" is the individual arterial systolic pressure after adrenaline injection $(2 \, \mu g \times kg^{-1})$. We choose to use systolic pressure to estimate the peak of the tensional forces experienced by the arteries during each cardiac cycle. Similarly, arterial wall stress was calculated as: $\sigma = T/W$. We also avoided the most curved sections of each arterial segment to minimize the effects of curvature on the calculation of wall tension in cylinders (Azuma and Oka 1974).

Utilizing the enhanced birefringent properties of Picro-Sirius red-stained collagen, polarization microscopy was used to estimate collagen content within the artery (Fig. 1d–f). Collagen content was assessed using pixel density analysis with ImageJ (Bautista and Burggren 2019). Briefly, bright-field and polarized light images from each tissue section were compared to calculate the total cross-sectional area of tissue. Bright-field images (Fig. 1b) were used

to calculate total cross-sectional area of tissue in the region of interest using a hue ratio of 0:255, saturation 30:255, and brightness 10:255. Polarized light images (Fig. 1e) were then used to assess collagen content, evident at a hue ratio of 0:105, saturation 0:255, and brightness 60:255. The relative amount of collagen per tissue was given as the ratio of collagen content identified by polarization microscopy (Fig. 1e), over the total cross-sectional area of tissue found at the bright-field analysis (Fig. 1b).

Statistical analysis

Scaling patterns were assessed using a non-linear power regression (equation: $Y = aX^b$) using body mass (kg) as the predicting variable. Variables that fit to a power regression were then log₁₀-transformed for comparisons of the scaling patterns between control values and after adrenaline injection $(f_H, Pm_{sys}, Ps_{sys}, Pm_{pul}, and Ps_{pul})$, or between RAo and LPA $(r_i, T, W, \sigma, \text{ and collagen content})$ with an analysis of covariance (ANCOVA) using $M_{\rm h}$ as the covariate. When data did not fit to a power regression (i.e., did not scale with $M_{\rm b}$), comparisons were made with a paired Student's T test for the hemodynamic variables, and a Student's T test for the morphological and mechanical variables. Non-linear power regressions were fitted with Sigma Plot v.11; we used Graph-Pad Prism version 7.00 for ANCOVAs, Student's T test, and graphs. Statistical significance was assigned as P < 0.05. All data are presented as mean $\pm 95\%$ CI.

Results

Heart mass and hemodynamic variables

Heart mass increased with $M_{\rm h}$, but as evident from the scaling factor being less than 1, the relative size of the heart decreased with M_b ($R^2 = 0.89$; P = 0.0001; $a = 2.51 \pm 0.88$; $b=0.78\pm0.22$; Fig. 2a). Heart rate decreased with increased

 $M_{\rm b}$ at control conditions and after adrenaline injection (Table 1; Fig. 2b). Although adrenaline exerted an excitatory chronotropic effect, the scaling factors remained similar (Table 1). Both mean and systolic arterial pressures from the systemic circulation increased with M_b (Table 1; Fig. 3a and b, respectively). Similar scaling factors persisted after adrenaline injection, although both mean and systolic arterial pressures were elevated (Table 1). Neither mean nor systolic pulmonary arterial pressures varied with $M_{\rm b}$ (Table 1), although adrenaline injection raised both parameters (Pm_{pul}: t = 10.57; P < 0.0001; Fig. 3c; Ps_{pul} : t = 15.26; P < 0.0001; Fig. 3d).

Arterial morphology and mechanics

The internal luminal radius of the RAo increased proportionally less than LPA (Table 2). The figures also indicate that the internal radius from RAo was larger than LPA (Fig. 4a). Wall tension was also higher in the RAo than the LPA, albeit with a similar scaling pattern (Table 2; Fig. 4b).

The wall thickness from RAo was larger than that of LPA, but both circuits scaled similarly with $M_{\rm b}$ (Table 2; Fig. 4c). The concomitant changes of wall thickness with tension caused stress to be independent of M_b for both RAo and LPA (Table 2), albeit differences between wall stress from RAo and LPA were statistically significant (t=-4.58; P=0.0001; Fig. 4d). Likewise, collagen content was independent from $M_{\rm b}$ for both RAo and LPA (Table 2). Both arteries displayed similar collagen contents (t=-0.72; P=0.48; Fig. 4e).

Discussion

This study was designed to investigate putative anatomical changes in the major systemic and pulmonary arterial vessels to resist the increased tensional forces as alligators grow larger. Our findings indicate that the thickening of the arterial walls as the alligators increased body mass occur

0

4

 ∞

O Control

Adrenaline

Fig. 2 Scaling of heart mass and heart rate in the American alligator, Alligator mississippiensis. Scaling patterns followed a non-linear power regression $(Y=aX^b)$. **a** Heart mass (g); **b** heart rate (bpm). Data for control values are represented by open circles and dashed lines; data for adrenaline injection are represented by closed circles and continuous line (n = 14)

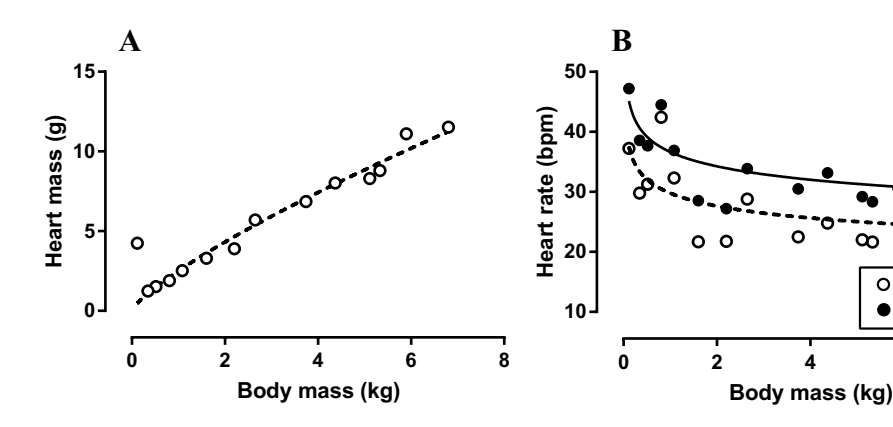




Figure 1. Allometric equations $(Y = aX^b)$ for scaling of hemodynamic variables at control conditions and after adrenaline injection in Alligator mississippiens is

Variable	Control				Adrenaline	ine			ANCOVA	
	R^2	Р	a	<i>q</i>	R^2	Р	a	p q	Slope	Intercept
$f_{ m H}$	0.38	0.019	29.79 ± 2.92	-0.11 ± 0.08	0.49	0.005	36.66 ± 2.55	-0.09 ± 0.06	$F_{1,25} = 0.92; P = 0.76$	$F_{1.25} = 0.92; P = 0.76$ $F_{1.26} = 14.13; P = 0.0009$
$P_{ m m_{ m sys}}$	0.55	0.002	2.13 ± 0.37	0.21 ± 0.12	0.74	< 0.0001	3.13 ± 0.33	0.20 ± 0.08	$F_{1,25} = 0.12; P = 0.73$	$F_{1.26} = 36.90$; $P < 0.00001$
$P_{ m s_{ m sys}}$	0.52	0.004	2.99 ± 0.47	0.19 ± 0.12	0.76	< 0.0001	4.63 ± 0.41	0.18 ± 0.06	$F_{1.25} = 0.04$; $P = 0.84$	$F_{1.26} = 55.47$; $P < 0.00001$
$P_{ m m_{ m pul}}$	0.14	0.20	1.01 ± 0.09	-0.05 ± 0.07	0.16	0.16	1.65 ± 0.13	-0.05 ± 0.06	. 1	. 1
$P_{ m S_{ m pul}}$	0.17	0.15	1.60 ± 0.14	-0.05 ± 0.07	0.13	0.21	2.85 ± 0.19	-0.04 ± 0.05	I	ı

Heart rate ($f_{\rm H}$; bpm), mean systemic arterial pressure ($P_{\rm sys}$; kPa), systemic systolic pressure ($P_{\rm sys}$; kPa), mean pulmonary arterial pressure ($P_{\rm mul}$; kPa), pulmonary systolic pressure ($P_{\rm sys}$; kPa). Data are presented as mean $\pm 95\%$ CI (n = 14). Differences between control and adrenaline injection regarding slopes and intercepts from \log_{10} -transformed data were tested with analysis of covariance (ANCOVA) without changes in relative collagen content. However, wall thickening was sufficient to offset the larger arterial internal radius and pressure, thus, normalizing wall stress at both circuits.

Scaling of heart mass confirmed previous observations (Altimiras et al. 2017), and indicates that the relative size of the heart, and thus, stroke volume, decreases with $M_{\rm b}$ (Schmidt-Nielsen 1984). The reduction in heart rate also agrees with previous studies in mammals, birds, and reptiles (Seymour 1987; Seymour and Blaylock 2000; Enok et al. 2014), and is usually attributed to a concomitant decrease in mass-specific metabolism (Dawson 2001). As in mammals (Baudinette 1978), adrenaline did not affect the heart rate scaling pattern. The increase of mean and systolic blood pressures from the systemic circulation with $M_{\rm b}$ agrees with previous studies on reptiles (Seymour 1987; Enok et al. 2014), although mean and systolic pulmonary blood pressures remained unchanged.

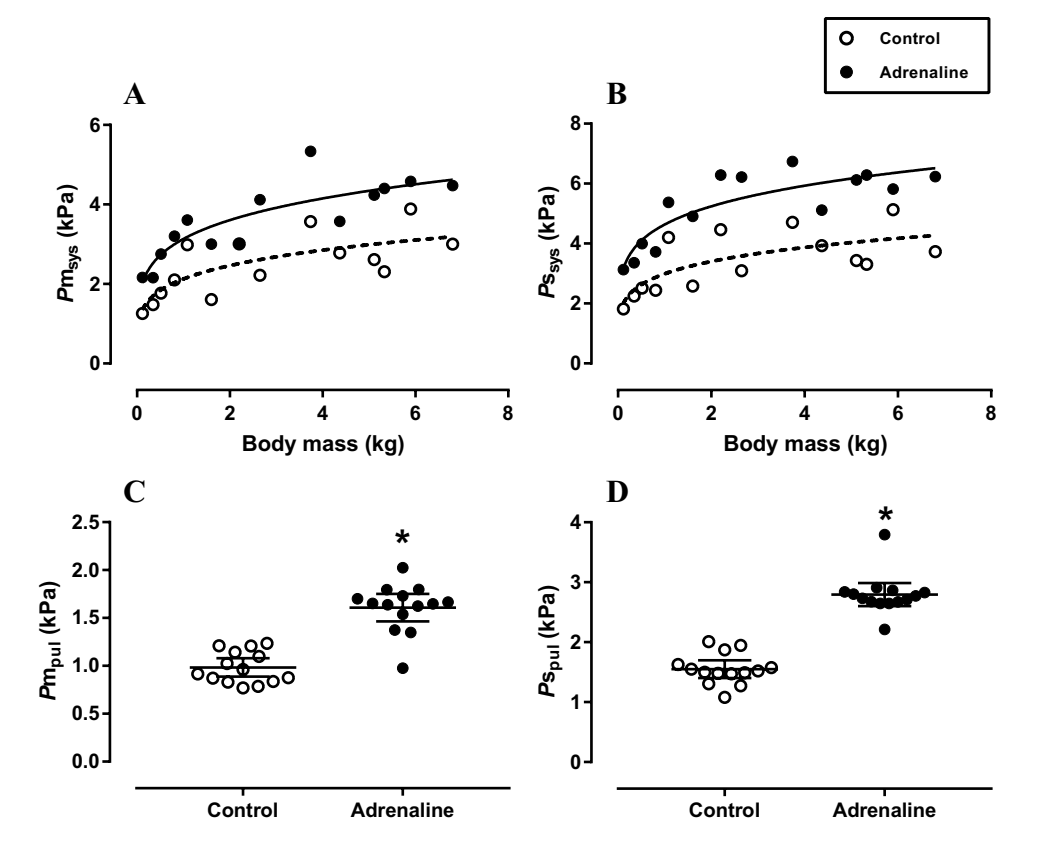
We acknowledge that anesthesia may depress the cardiovascular system (Vatner and Braunwald 1975; Çeçen et al. 2009; Filogonio et al. 2014), and while the pressures recorded in anesthesia may differ from recovered animals, there is no a priori reason to believe that such an effect should differ with body mass. During the present study, mean heart rate recorded after adrenaline injection was similar to values observed for recovered A. mississippiensis during activity (30-40 bpm—Joyce et al. 2018). Although mean systemic arterial pressures were reduced, the systolic blood pressure of the systemic circulation—which in this study was utilized to calculate arterial wall tension and stress—was similar to mean systemic arterial pressures from recovered crocodilians (e.g. ~ 3 kPa for hatchling A. mississippiensis – Crossley et al. 2003; 5.10 ± 0.39 kPa in Caiman *latirostris* weighting 1.81 ± 0.27 kg—Hagensen et al. 2010; and 7.10 ± 1.57 kPa in *Crocodylus porosus* with a mean body mass of 2.02 ± 0.12 kg—Altimiras et al. 1998). The goal of the adrenaline treatment was to elevate arterial pressures within a physiologically relevant range that might be experienced by the arterial tree. Although adrenergic stimulation may affect the vascular tone of the systemic and pulmonary conduit and resistance vessels (Campos et al. 2019; Filogonio et al. 2020), vascular resistance is essentially regulated downstream, at the level of small arteries and arterioles (Mulvany and Aalkjaer 1990). Since injection of adrenaline elevated systolic blood pressures to similar values to mean blood pressure recorded in recovered crocodilians, calculated wall tension and stress were physiologically relevant.

Arterial morphology and mechanics

Wall tension was higher in the RAo compared to the LPA. In a recent study of the yellow anaconda, *Eunectes notaeus*, the systemic dorsal artery was more elastic than the pulmonary



Fig. 3 Scaling of the systemic and pulmonary hemodynamic parameters of the American alligator, Alligator mississippiensis. The scaling pattern followed a non-linear power regression $(Y=aX^b)$. Data for control values are represented by open circles and dashed lines; data for adrenaline injection are represented by closed circles and continuous line. a Mean systemic arterial pressure (kPa); **b** systemic systolic pressure (kPa); c mean pulmonary arterial pressure (kPa); d pulmonary systolic pressure (kPa). In c and d, data are presented as mean ±95% CI and statistical differences are represented by an asterisk (n = 14)



artery (Filogonio et al. 2018). If A. mississippiensis exhibits similar arterial mechanical properties, then the higher wall tension experienced by the RAo may be beneficial, since it would improve the arterial recoil during the diastolic phase (i.e., the Windkessel effect). Since the systemic circulation typically exhibits a higher peripheral resistance than the pulmonary circulation (Barnes and Liu 1995), larger wall tensions could improve the recoiling function of the distended arterial wall to overcome this elevated afterload. This mechanism could be further enhanced for both circuits at larger body sizes since lower heart rate results in a longer diastolic phase (Westerhof and Elzinga 1991); the time of pressure decay scales with size and is proportional to pulse interval in mammals (Westerhof and Elzinga 1991). In this context, the increased wall tension could sustain arterial recoiling for longer periods, thus, ensuring constant blood flow for larger animals even at reduced heart rate.

As demonstrated, the increase in wall thickness was sufficient to normalize tension, rendering wall stress independent of $M_{\rm h}$ in both arteries. A similar adaptation has been

observed in the left ventricular wall of the giraffe, *Giraffa camelopardalis*, which experiences a disproportional thickening to resist elevated blood pressures as individuals grow (Smerup et al. 2016). The arterial wall of mammals also increases with size and the resultant stress is reduced (Prim et al. 2018). Therefore, wall thickening seems to be a convergent mechanism within the cardiovascular system of vertebrates to resist increased tensional forces.

Although the arterial wall from the RAo was thicker, the stress experienced by this artery was higher than the LPA. Therefore, we expected the RAo collagen content would be higher than in the LPA, but this hypothesis was refuted. In the ball python, *Python regius*, a reptile with functional ventricular separation, although maximum stress recorded for both systemic and pulmonary circuits were similar, the pulmonary artery experienced larger stress at lower relative stretch (van Soldt et al. 2015). Therefore, our results may indicate that the systemic circuit is subjected to a much larger strain than the pulmonary artery in *A. mississippiensis*. Alternatively, in *E. notaeus*, the systemic artery possessed collagen capable of



in Alligator mississippiensis **Table 2** Allometric equations $(Y = aX^b)$ for the scaling of morphological and mechanical variables from the right aortic arch and the left pulmonary

Variable	Right aortic arch	rtic arch			Left puln	Left pulmonary artery			ANCOVA	
	R ²	Р	a	<i>p</i>	R^2	Р	a	<i>q</i>	Slopes	Intercepts
$r_{\rm i}$	0.34	0.035	1.09 ± 0.22	0.16 ± 0.14 0.74	0.74	0.0003	0.44±1.18	0.40 ± 0.18	$F_{1,22} = 5.32; P = 0.03$. 1
T	0.70	0.0003	4.97 ± 1.23	0.35 ± 0.18	0.78	0.0001	1.17 ± 0.29	0.42 ± 0.18	$F_{1.22} = 0.55$; $P = 0.47$	$F_{1.22} = 0.55$; $P = 0.47$ $F_{1.23} = 163.27$; $P < 0.000001$
W	0.32	0.045	0.26 ± 0.10	0.24 ± 0.24	0.36	0.041	0.18 ± 0.06	0.25 ± 0.24	$F_{1,22} = 0.02$; $P = 0.89$ $F_{1,23} = 7.06$; $P = 0.01$	$F_{1.23} = 7.06; P = 0.01$
ο	0.0003	96.0	24.35 ± 8.19	0.008 ± 0.25	0.15	0.22	7.07 ± 3.10	0.19 ± 0.32	. 1	. 1
Collagen content	0.02	0.69	47.63 ± 8.04	0.03 ± 0.12	0.0005	0.95	44.26 ± 8.66	0.005 ± 0.15	I	1

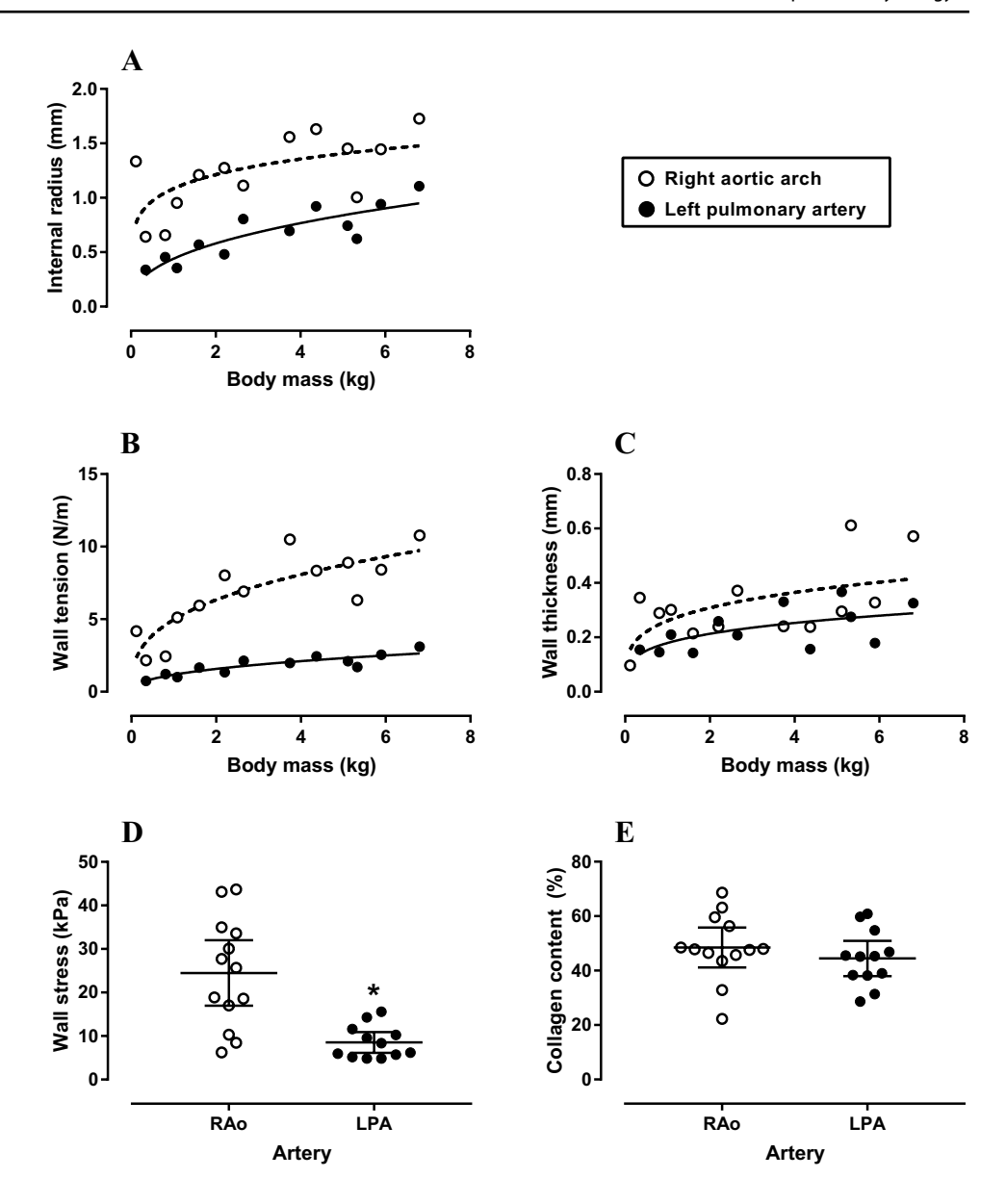
Internal radius $(r_i; mm)$, wall tension (T; N/m), wall thickness (W; mm), wall stress $(\sigma; RPa)$, and collagen content (%). Data are presented as mean $\pm 95\%$ CI (n=13 for RAo; n=12 for LPA)Differences between the right aortic arch and the left pulmonary artery regarding slopes and intercepts from log₁₀-transformed data were tested with analysis of covariance (ANCOVA) tolerating higher loads than the pulmonary artery (Filogonio et al. 2018). This can be attributed to different collagen isoforms, fiber orientation and crosslinking, or the interplay with other components of the extracellular matrix, such as elastin and glycosaminoglycans (Dingemans et al. 2000; MacDonald et al. 2000; Humphrey 2008; Wagenseil and Mecham 2009). Therefore, it is possible that intrinsic collagen properties differ between the RAo and the LPA in *A. mississippiensis*, as in *E. notaeus* (Filogonio et al. 2018). As such, it is likely that the collagen matrix arrangement, differential ratios of collagen isoforms and other extracellular matrix proteins may be contributing to resist the increase in arterial wall tension in larger body sizes.

Conclusions

In the present study, heart rate decreased with $M_{\rm b}$, agreeing with previous studies on reptiles. The increase of systolic and mean systemic blood pressures with size was not paralleled by systolic and mean pulmonary blood pressures. The internal luminal radius from both RAo and LPA increased with $M_{\rm b}$, which led to increased wall tension at both arteries. The relative content of collagen did not scale with animal size and the different wall stress between RAo and LPA indicates that these arteries are experiencing different strain, or that the collagen capacity needed to endure increasing tensional forces diverges between the systemic and pulmonary circuits. Normalization of wall tension was attained with the scaling of the wall thickness at both RAo and LPA, rendering wall stress independent of $M_{\rm b}$. Thus, it appears that the scaling of the wall thickness allows growing alligators to resist artery rupture from increasing tensions.



Fig. 4 Scaling of morphological and mechanical parameters of the right aortic arch and the pulmonary artery of the American alligator, Alligator mississippiensis. The scaling pattern followed a non-linear power regression $(Y = aX^b)$. Data for the right aortic arch (RAo) values are represented by open circles and dashed lines: data for the left pulmonary artery (LPA) are represented by closed circles and continuous line. a Internal radius (mm); **b** wall tension (N/m): **c** wall thickness (mm); d wall stress (kPa); e collagen content (%). In d and e, data are presented as mean ±95% CI and statistical differences are represented by an asterisk (n = 14)



Acknowledgements We thank Janna Crossley, Kevin Stewart, Amanda Reynolds, and Brandt Smith for caring of the alligators. Janna Crossley and Brandt Smith also helped during the experiments, and Andrea Bernardino-Schaefer provided microscopy and imaging support.

Author contributions RF, TW, CACL, and DAC conceived the study. RME provided resources and specimens. RF, BDD and BHD collected and analyzed the data. RF wrote the manuscript, and all the authors approved the final version of the manuscript.

Funding RF received a postdoctoral grant from São Paulo Research Foundation (FAPESP, process #2016/20158-6); BDD was financed by World Precision Instruments, LLC. and the UNT College of Science Seed Grant; BHD was financed by Tarleton State University Office of Research and Innovation; CACL had financial support from FAPESP (process #2018/05035-0); TW was supported by the Danish Council for Independent Research, Natural Sciences (Det Frie Forskningsråd | Natur og Univers, FNU). DAC II had financial support from National Science Foundation (NSF) and a Career Award IBN IOS-0845741.

References

Altimiras J, Franklin CE, Axelsson M (1998) Relationships between blood pressure and heart rate in the saltwater crocodile *Crocodylus porosus*. J Exp Biol 201:2235–2242

Altimiras J, Lindgren I, Giraldo-Deck LM et al (2017) Aerobic performance in tinamous is limited by their small heart. A novel hypothesis in the evolution of avian flight. Sci Rep 7:15964. https://doi.org/10.1038/s41598-017-16297-2

Alves AC, de Ribeiro CLDB, Cotrin JV et al (2016) Descrição morfológica do coração e dos vasos da base do jacaré-do-pantanal (*Caiman yacare* Daudin, 1802) proveniente de zoocriadouro. Pesqui Vet Bras 36:8–14. https://doi.org/10.1590/S0100-736X2 016001300002

Avery RA (1994) Growth in reptiles. Gerontology 40:193–199. https://doi.org/10.1159/000213587

Axelsson M, Franklin CE, Löfman CO et al (1996) Dynamic anatomical study of cardiac shunting in crocodiles using high-resolution angioscopy. J Exp Biol 199:359–365



- Azuma T, Oka S (1974) Circumferential tension in the wall of bent blood vessels. Microvasc Res 7:10–18. https://doi.org/10.1016/0026-2862(74)90033-8
- Barnes PJ, Liu SF (1995) Regulation of pulmonary vascular tone. Pharmacol Rev 47:87–131
- Baudinette RV (1978) Scaling of heart rate during locomotion in mammals. J Comp Physiol B 127:337–342. https://doi.org/10.1007/BF00738418
- Bautista NM, Burggren WW (2019) Parental stressor exposure simultaneously conveys both adaptive and maladaptive larval phenotypes through epigenetic inheritance in the zebrafish (*Danio rerio*). J Exp Biol 222:jeb208918, https://doi.org/10.1242/jeb.208918
- Campos R, Justo AFO, Jacintho FF et al (2019) Pharmacological and transcriptomic characterization of the nitric oxide pathway in aortic rings isolated from the tortoise *Chelonoidis carbonaria*. Comp Biochem Physiol Part C Toxicol Pharmacol 222:82–89. https:// doi.org/10.1016/j.cbpc.2019.04.015
- Çeçen G, Topal A, Sacit O, Akgöz S (2009) The cardiopulmonary effects of sevoflurane, isoflurane and halothane anesthesia during spontaneous or controlled ventilation in dogs. Ank Üniv Vet Fak Derg 50:255–261. https://doi.org/10.1501/Vetfak_0000002291
- Cook AC, Tran V-H, Spicer DE et al (2017) Sequential segmental analysis of the crocodilian heart. J Anat 231:484–499. https://doi. org/10.1111/joa.12661
- Cox RH (1978) Comparison of carotid artery mechanics in the rat, rabbit, and dog. Am J Physiol Heart Circ Physiol 234:H280–H288. https://doi.org/10.1152/ajpheart.1978.234.3.H280
- Crossley DA, Hicks JW, Altimiras J (2003) Ontogeny of baroreflex control in the American alligator *Alligator mississippiensis*. J Exp Biol 206:2895–2902. https://doi.org/10.1242/jeb.00486
- Dawson TH (2001) Similitude in the cardiovascular system of mammals. J Exp Biol 204:395–407
- Dingemans KP, Teeling P, Lagendijk JH, Becker AE (2000) Extracellular matrix of the human aortic media: an ultrastructural histochemical and immunohistochemical study of the adult aortic media. Anat Rec 258:1–14. https://doi.org/10.1002/(SICI)1097-0185(20000101)258:1%3c1::AID-AR1%3e3.0.CO;2-7
- Dubansky BH, Dubansky BD (2018) Natural development of dermal ectopic bone in the American alligator (*Alligator mississippiensis*) resembles heterotopic ossification disorders in humans. Anat Rec 301:56–76. https://doi.org/10.1002/ar.23682
- Enok S, Slay C, Abe AS et al (2014) Intraspecific scaling of arterial blood pressure in the Burmese python. J Exp Biol 217:2232–2234. https://doi.org/10.1242/jeb.099226
- Ferguson MWJ (1985) Reproductive biology and embryology of the crocodilians. Biology of the Reptilia, vol 14, Development A. Wiley, New York, pp 329–491
- Filogonio R, Crossley DA II (2019) Long term effects of chronic prenatal exposure to hypercarbia on organ growth and cardiovascular responses to adrenaline and hypoxia in common snapping turtles. Comp Biochem Physiol A Mol Integr Physiol 234:10–17. https://doi.org/10.1016/j.cbpa.2019.04.009
- Filogonio R, Taylor EW, Carreira LBT et al (2014) Systemic blood flow relations in conscious South American rattlesnakes. S Am J Herpetol 9:171–176. https://doi.org/10.2994/SAJH-D-14-00012.1
- Filogonio R, Wang T, Danielsen CC (2018) Analysis of vascular mechanical properties of the yellow anaconda reveals increased elasticity and distensibility of the pulmonary artery during digestion. J Exp Biol 221:jeb177766. https://doi.org/10.1242/jeb.177766
- Filogonio R, Wang T, Abe AS, Leite CAC (2019) Cooling and warming rates are unaffected by autonomic vascular control in the South American rattlesnake (*Crotalus durissus*). S Am J Herpetol 14:242–249. https://doi.org/10.2994/SAJH-D-18-00013.1
- Filogonio R, Sartori MR, Mogensen S et al (2020) Cholinergic regulation along the pulmonary arterial tree of the South American rattlesnake: vascular reactivity, muscarinic receptors, and vagal innervation. Am

- J Physiol Regul Integr Comp Physiol 319:R156–R170. https://doi.org/10.1152/ajpregu.00310.2019
- Galli GLJ, Skovgaard N, Abe AS et al (2007) The adrenergic regulation of the cardiovascular system in the South American rattlesnake, *Crotalus durissus*. Comp Biochem Physiol A Mol Integr Physiol 148:510–520. https://doi.org/10.1016/j.cbpa.2007.06.420
- Greenfield JC, Griggs DM (1963) Relation between pressure and diameter in main pulmonary artery of man. J Appl Physiol 18:557–559. https://doi.org/10.1152/jappl.1963.18.3.557
- Greenfield JC, Patel DJ (1962) Relation between pressure and diameter in the ascending aorta of man. Circ Res 10:778–781. https://doi.org/10.1161/01.RES.10.5.778
- Hagensen MK, Abe AS, Wang T (2010) Baroreflex control of heart rate in the broad-nosed caiman *Caiman latirostris* is temperature dependent. Comp Biochem Physiol A Mol Integr Physiol 156:458–462. https://doi.org/10.1016/j.cbpa.2010.03.028
- Holt JP, Rhode EA, Holt WW, Kines H (1981) Geometric similarity of aorta, venae cavae, and certain of their branches in mammals. Am J Physiol Regul Integr Comp Physiol 241:R100–R104. https://doi. org/10.1152/ajpregu.1981.241.1.R100
- Humphrey JD (2008) Mechanisms of arterial remodeling in hypertension: coupled roles of wall shear and intramural stress. Hypertension 52:195–200. https://doi.org/10.1161/HYPERTENSIONAHA.107.103440
- Joyce W, Miller TE, Elsey RM et al (2018) The effects of embryonic hypoxic programming on cardiovascular function and autonomic regulation in the American alligator (*Alligator mississippiensis*) at rest and during swimming. J Comp Physiol B 188:967–976. https:// doi.org/10.1007/s00360-018-1181-2
- Lima MO, Nóbrega YC, Santos MRD et al (2020) Notes on the gross anatomy of the heart of the broad-snouted caiman, *Caiman latiro*stris (Daudin, 1802). Anat Histol Embryol. https://doi.org/10.1111/ ahe.12636
- MacDonald DJ, Finlay HM, Canham PB (2000) Directional wall strength in saccular brain aneurysms from polarized light microscopy. Ann Biomed Eng 28:533–542. https://doi.org/10.1114/1.292
- Mulvany MJ, Aalkjaer C (1990) Structure and function of small arteries. Physiol Rev 70:921–961. https://doi.org/10.1152/physrev.1990.70.4.921
- Nichols WW, O'Rourke MF, Vlachopoulos C (2011) McDonald's blood flow in arteries: theoretical, experimental and clinical principles, 6th edn. CRC Press, Boca Raton
- Poulsen CB, Wang T, Assersen K et al (2018) Does mean arterial blood pressure scale with body mass in mammals? Effects of measurement of blood pressure. Acta Physiol 222:e13010. https://doi.org/10.1111/apha.13010
- Prim DA, Mohamed MA, Lane BA et al (2018) Comparative mechanics of diverse mammalian carotid arteries. PLoS ONE 13:e0202123. https://doi.org/10.1371/journal.pone.0202123
- Schmidt-Nielsen K (1984) Scaling: why is animal size so important? Cambridge University Press, Cambridge
- Schneider CA, Rasband WS, Eliceiri KW (2012) NIH image to ImageJ: 25 years of image analysis. Nat Methods 9:671–675. https://doi.org/10.1038/nmeth.2089
- Seldinger SI (1953) Catheter replacement of the needle in percutaneous arteriography: a new technique. Acta Radiol 39:368–376. https://doi.org/10.3109/00016925309136722
- Seymour RS (1987) Scaling of cardiovascular physiology in snakes. Am Zool 27:97–109
- Seymour RS, Blaylock AJ (2000) The Principle of Laplace and scaling of ventricular wall stress and blood pressure in mammals and birds. Physiol Biochem Zool 73:389–405. https://doi.org/10.1086/317741
- Seymour RS, Hu Q, Snelling EP, White CR (2019) Interspecific scaling of blood flow rates and arterial sizes in mammals. J Exp Biol 222:jeb199554. https://doi.org/10.1242/jeb.199554



- Shadwick RE (1998) Elasticity in arteries: a similar combination of rubbery and stiff materials creates common mechanical properties in blood vessels of vertebrates and some invertebrates. Am Sci 86:535–541
- Smerup M, Damkjær M, Brøndum E et al (2016) The thick left ventricular wall of the giraffe heart normalises wall tension, but limits stroke volume and cardiac output. J Exp Biol 219:457–463. https://doi.org/10.1242/jeb.132753
- Smith B, Crossley JL, Elsey RM et al (2019) Embryonic developmental oxygen preconditions cardiovascular functional response to acute hypoxic exposure and maximal β-adrenergic stimulation of anesthetized juvenile American alligators (*Alligator mississippiensis*). J Exp Biol 222:jeb205419. https://doi.org/10.1242/jeb.205419
- van Soldt BJ, Danielsen CC, Wang T (2015) The mechanical properties of the systemic and pulmonary arteries of *Python regius* correlate with blood pressures. J Morphol 276:1412–1421. https://doi.org/10.1002/jmor.20429
- Vatner SF, Braunwald E (1975) Cardiovascular control mechanisms in the conscious state. N Engl J Med 293:970–976. https://doi.org/10.1056/ NEJM197511062931906
- Wagenseil JE, Mecham RP (2009) Vascular extracellular matrix and arterial mechanics. Physiol Rev 89:957–989. https://doi.org/10.1152/physrev.00041.2008

- West GB, Brown JH, Enquist BJ (1997) A general model for the origin of allometric scaling laws in biology. Science 276:122–126. https:// doi.org/10.1126/science.276.5309.122
- Westerhof N, Elzinga G (1991) Normalized input impedance and arterial decay time over heart period are independent of animal size. Am J Physiol Regul Integr Comp Physiol 261:R126–R133. https://doi.org/10.1152/ajpregu.1991.261.1.R126
- White FN (1976) Circulation. Biology of the Reptilia 5, physiology A. Academic, New York, pp 275–334
- White CR, Seymour RS (2014) The role of gravity in the evolution of mammalian blood pressure. Evolution 68:901–908. https://doi.org/10.1111/evo.12298
- Wolinsky H, Glagov S (1967) A lamellar unit of aortic medial structure and function in mammals. Circ Res 20:99–111. https://doi.org/10.1161/01.RES.20.1.99

Publisher's Note Springer Nature remains neutral with regard to jurisdictional claims in published maps and institutional affiliations.

